Available online at www.sciencedirect.com
SCIENCE DIRECT®
Journal of Organometallic Chemistry 690 (2005) 1456–1466
Journal of Organometallic Chemistry
www.elsevier.com/locate/jorganchem

Reactivity of silyl-substituted heterobimetallic iron–platinum hydride complexes towards unsaturated molecules: Part II. Insertion of trifluoropropyne and hexafluorobutyne into the platinum–hydride bond

Michael Knorr [a,*], Isabelle Jourdain [a], Fernando Villafañe [b], Carsten Strohmann [c]

[a] *Laboratoire de Chimie des Matériaux et Interfaces, Université de Franche-Comté, Faculté des Sciences et des Techniques, 16, Route de Gray, F-25030 Besançon Cédex, France*
[b] *Química Inorgánica, Facultad de Ciencias Universidad de Valladolid, 47005 Valladolid, Spain*
[c] *Institut für Anorganische Chemie der Universität Würzburg, Am Hubland, D-97074 Würzburg, Germany*

Received 10 June 2004; accepted 23 November 2004
Available online 26 January 2005

Abstract

Insertion of hexafluorobutyne into the Pt–H bond of the heterobimetallic complexes $[(OC)_3Fe\{Si(OMe)_3\}(\mu\text{-}Ph_2PXPPh_2)Pt(H)(PPh_3)]$ (**1a** X = CH_2; **1b** X = NH) yields the σ-alkenyl complexes $[(OC)_3Fe\{\mu\text{-}Si(OMe)_2(OMe)\}(\mu\text{-}Ph_2PXPPh_2)Pt\{C(CF_3)=C(H)CF_3\}]$ (**3a** X = CH_2; **3b** X = NH). This insertion reaction is accompanied by dissociation of the platinum bound PPh_3 ligand and saturation of the vacant coordination site by a dative $\mu-\eta^2$-Si–O → Pt interaction. Addition of the Pt–H bond of **1a** across the triple bond of 3,3,3-trifluoropropyne affords in a regiospecific manner $[(OC)_3Fe\{\mu\text{-}Si(OMe)_2(OMe)\}(\mu\text{-dppm})Pt\{C(CF_3)=CH_2\}]$ (**2**) having the trifluoromethyl substituent on the α-carbon. Addition of RN≡C to **3** affords the isocyanide adducts $[(OC)_3Fe\{Si(OMe)_3\}(\mu\text{-}Ph_2PXPPh_2)Pt(CNR)\{C(CF_3)=C(H)CF_3\}]$ (**4a** R = *t*-Bu, X = CH_2; **4b** R = 2,6-xylyl, X = CH_2; **4c** R = 2,6-xylyl, X = NH). In dichloromethane solution **3a** is gradually transformed into the C_4F_6-bridged compound $[(OC)_3Fe(\mu\text{-dppm})(\mu\text{-}CF_3C=CCF_3)Pt(CO)]$ **5**. The Pt-bound carbonyl ligand of **5** is displaced by xylylisocyanide or trimethylphosphite affording the derivatives $[(OC)_3Fe(\mu\text{-dppm})(\mu\text{-}CF_3C=CCF_3)Pt(CNxylyl)]$ **6** and $[(OC)_3Fe(\mu\text{-dppm})(\mu\text{-}CF_3C=CCF_3)Pt\{P(OMe)_3\}]$ **7**. The molecular structures of **4a**, **5** and **6** have been determined by X-ray diffraction studies.

Keywords: Heterobimetallics; Hydride; Alkenyl complexes; Insertion; Alkyne; Iron; Platinum

1. Introduction

Owing to a rich reactivity, the coordination and activation of alkynes at heterodinuclar complexes still attracts considerable attention [1]. Apart from simple ligand displacement reactions in the coordination sphere of the bimetallic system [2], oxidative addition of terminal alkynes may lead to alkynyl compounds [3]. The formation of metallacyclobutenones or metallacylopentenones via carbon–carbon coupling reactions with carbonyl ligands is well documented [2,4,5]; further examples for carbon–carbon bond formation are coupling reactions with bridging carbyne ligands [6] or head to head alkyne coupling across a Fe–Rh or Mo–Co unit [7]. Another reactivity pattern are insertion reactions in metal–metal [8], metal–phosphorus [9,10], metal–carbon [11,12] and metal–hydride bonds. Examples for the latter reaction are the insertion of alkynes in the Os–H and Rh–H of $[(OC)Rh(\mu\text{-dppm})_2Os(H)$-

* Corresponding author. Fax: +33 381 666 438.
E-mail address: michael.knorr@univ-fcomte.fr (M. Knorr).

0022-328X/$ - see front matter © 2004 Elsevier B.V. All rights reserved.
doi:10.1016/j.jorganchem.2004.11.052

$(CO)_2$] and [(OC)Rh(μ-dppm)$_2$Mo(μ-H)$(CO)_3$] generating σ-alkenyl complexes [13]. Note that addition of alkynes to the hydride compound [(η^5-Cp)$(OC)_3$Mo–Pt(H)(dppe)] promotes first hydrogen transfer with concomittant cleavage of the metal–metal bond [14]. Only in case of terminal alkynes, subsequent addition of [(η^5-Cp)$(OC)_3$Mo(H)] across [(HC≡CR)Pt(dppe)] generates the final alkenyl-bridged system [(η^5-Cp)$(OC)_2$-Mo(μ-CO)(μ-H_2C=CR)Pt(H)(dppe)].

In the course of our investigations on the activation of small molecules by heterobimetallics, we recently examined the insertion of phenylacetylene and *p*-tolylacetylene into the Pt–H bond of heterodinuclear iron–platinum hydride complexes [$(OC)_3$Fe{Si$(OMe)_3$}(μ-Ph_2PXPPh_2)Pt(H)(PPh_3)] (**1a** X = CH_2; **1b** X = NH) [15]. The influence of the second adjacent metal center close to a square planar platinum(II) moiety on the regio- and site selectivity of this important reaction was of special interest. We found that insertion of these aromatic terminal alkynes afforded first the isolable σ-alkenyl complexes [$(CO)_3$Fe{μ-Si$(OMe)_2$(OMe)}(μ-Ph_2PXPPh_2)Pt{(Ar)C=CH_2}], which were transformed in a subsequent rearrangement reaction in the presence of PPh_3 into the stable μ-vinylidene complexes [$(OC)_3$-Fe{μ-C=C(H)Ar}(μ-Ph_2PXPPh_2)Pt(PPh_3)] (Scheme 1).

In order to evaluate the influence of a strongly electron-withdrawing CF_3 substituent on the outcome of the reaction, we have studied the reactivity of **1** towards the activated alkynes 3,3,3-trifluoropropyne and hexafluorobut-2-yne. We report here on the synthesis of σ-alkenyl complexes, as well on their transformation to structurally characterized isocyanide adducts and intermolecular formation of μ-F_3CC=CCF_3 Fe–Pt complexes.

2. Results and discussion

2.1. Reactivity of *1* towards trifluoropropyne

Trifluoropropyne was condensed into a frozen CH_2Cl_2 solution of **1a**. After reaching ambient temperature, rapid insertion across the triple bond took place. After work-up, yellowish [$(OC)_3$Fe{μ-Si$(OMe)_2$-(OMe)}(μ-dppm)Pt{C(CF_3)=CH_2}] (**2**) was isolated in 88% yield (Scheme 2).

According to the proton NMR spectrum, a coordination site on the platinum centre is electronically saturated by a dative interaction of a methoxy group of the trimethoxysilyl ligand forming a four-membered Fe–Si–O → Pt cycle, since two singlets in a 2:1 ratio at δ 3.78 and 3.69 due to non-equivalent SiOMe groups are observed. The two geminal alkenyl hydrogens show no resolved mutual couplings; the broadened singlet at δ 6.01 displaying a strong ^3J(Pt–H) coupling of 121 Hz is assigned to the (*E*)-proton in *trans*-position relative to platinum, due to a weaker ^3J(Pt–H) coupling of 64 Hz the second vinylic resonance at δ 4.91 is assigned to

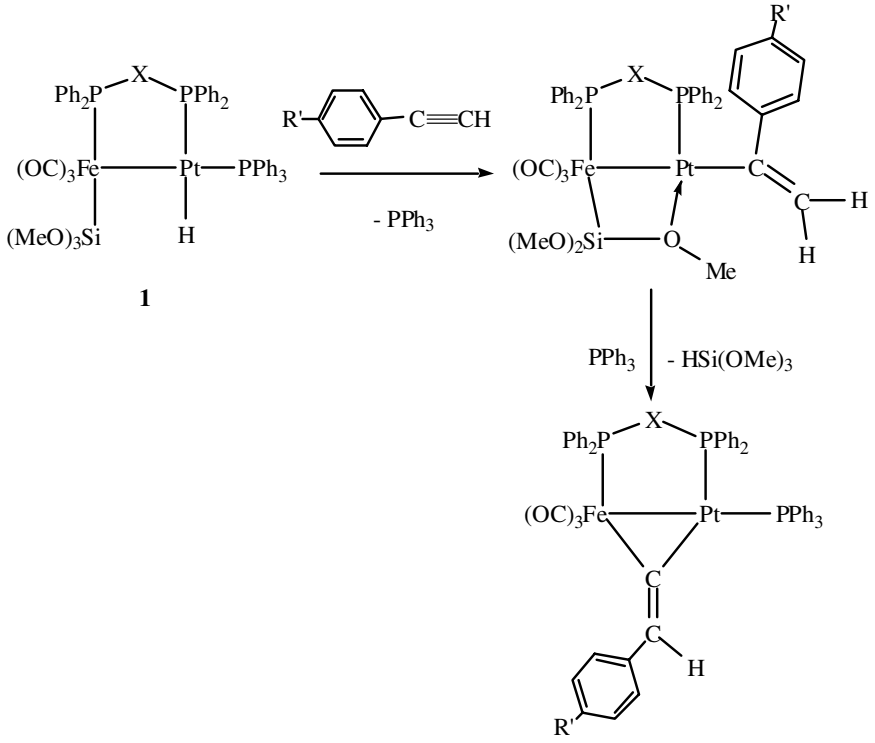

Scheme 1.

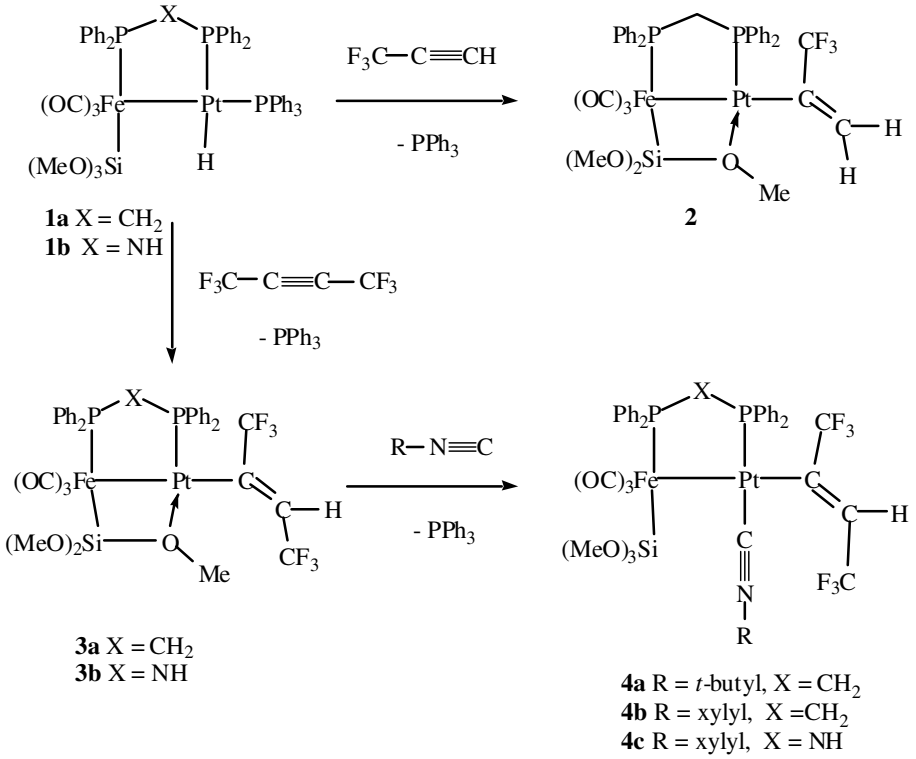

Scheme 2.

the (*Z*)-proton. Further support for the regiochemistry about the alkenyl ligand is provided by the $^{19}F\{^1H\}$ spectrum, where a singlet occurs at δ −59.9. Comparison of the ^3J(Pt–F) coupling constant (61 Hz) with that reported for *cis*-[$(PEt_3)_2$(Cl)Pt{$C(CF_3)$=CH_2}] (72 Hz) [16] indicates that the trifluoromethyl group is situated at the α-carbon of the alkenyl ligand. The $^{195}Pt\{^1H\}$ NMR spectrum consists of a doublet of multiplets centred at δ −2367.1. A simulation with the g-NMR software package confirms the experimental pattern with a large ^1J(Pt–P) coupling of 4898 Hz, a weak ^{2+3}J(Pt–P) coupling of 43 and an additional ^3J(Pt–F) coupling of 61 Hz. In the ^{29}Si-INEPT NMR spectrum no resolved long-range ^5J(Si–F) coupling is detectable, the doublet of doublets pattern at δ 16.75 stems from a ^2J(P–Si) and ^3J(P–Si) coupling of 34.5 and 4.4 Hz, respectively.

2.2. Reactivity of *1* towards hexafluorobutyne (HFB)

IR monitoring revealed that upon bubbling of a slow stream of the C_4F_6 through a CH_2Cl_2 solution of **1**, quantitative insertion occurred after 6 h leading to complexes [$(OC)_3$Fe{μ-Si$(OMe)_2$(OMe)}(μ-Ph_2PXPPh_2)Pt-{$C(CF_3)$=C(H)CF_3}] (**3a** X = CH_2; **3b** X = NH). According to microanalysis and the ^{31}P NMR data, the crystalline sample of **3b** isolated in 47% yield forms an adduct with one molecule of triphenylphosphane oxide via a N–H···O=PPh_3 hydrogen bond. This oxidation of PPh_3 occurred probably by intrusion of O_2 during purging with hexafluorobutyne and work-up. As exemplified for **3a**, these yellow stable complexes, which are soluble in toluene and halogenated solvents, possess a *trans*-configuration of the CF_3 substituents about the σ-alkenyl ligand. This follows from the ^{1}H NMR spectrum, where the vinylic proton gives rise to a complicated multiplet centred at δ 6.49 due to coupling with the two trifluoromethyl substituents. The magnitude of the ^3J(Pt–H) coupling of 116 Hz is indicative for a *trans* -position relative to platinum, in other words the stereochemistry about the C=C bond is *trans*. Again, a rigid four-membered Fe–Si–O → Pt cycle is formed via a dative interaction of a methoxy group of the trimethoxysilyl ligand; due to the dissymmetric environment around Pt, three distinct resonances for the methoxy groups are found at δ 3.72, 3.70 and 3.60, the latter being splitted in a doublet by a ^4J(P–H) coupling of 2 Hz.

The finding that insertion of hexafluorobutyne into the Pt–H bond of **1** occurs exclusively with a *trans*-stereochemistry about the resulting alkenyl complex needs some comments. By a labelling experiment using deuterated phenylacetylene, we have shown that the deuteron is located cis to Pt, consistent with a *cis*-addition of **1** across the Ph–C≡C–D triple bond [15]. In the case of alkyne insertion in Pt–H bonds, examples of both *cis* and *trans* insertions have been reported. Puddephatt has demonstrated that treatment of the dinuclear hydride [Pt_2H_2(μ-H)(μ-dppm)$_2$][PF_6] with dimethylacetylenedicarboxylate (DMAD) or HFB

in dichloromethane leads to $[Pt_2Cl\{CR{=}C(H)R\}(\mu\text{-}RC{=}CR)(\mu\text{-}dppm)_2]$ (R = CO_2Me, CF_3) with a *cis*-stereochemistry of R about the alkenyl ligand [17]. *cis*-insertion of diphenylacetylene in a μ-hydride bond has also been evidenced cristallographically for a Rh–Pt complex [13c]. Clark has reported that *cis*-insertion occurs upon treatment of *trans*-$[(PEt_3)PtH(acetone)][PF_6]$ with phenylmethylacetylene in acetone [18]. The migratory insertion reaction of *trans*-$[(PEt_3)PtH(Cl)]$ with HFB and DMAD in polar solvents such as methanol or acetone gives also alkenyl groups having *cis*-geometry, involving a 4-centered transition state [18]. However, using benzene as solvent, DMAD insertion proceeds with formation of mixtures of isomers having *cis* and *trans*-geometries about the alkenyl ligand [19]. A free-radical participation has been ascertained by ESR experiments in the presence of free-radical initiators. More recently, Steinborn has evidenced that reaction of MeS–C≡C-Ph with *trans*-$[(PEt_3)PtH(Cl)]$ both in benzene and methanol leads exclusively to *cis*-$[(PEt_3)PtCl\{E\text{-}(SMe)C{=}C(H)Ph\}]$ [20]. Since addition of radical inhibitors had no influence on the outcome of the reaction course, oxidative addition of MeS–C≡C–Ph leading to a Pt(IV) alkynyl species, subsequent 1,3 hydride shift and finally migration of a MeS ligand along a vinylidene intermediate have been proposed. These finding show that several parameters are decisive for the stereochemistry about the alkenyl ligand. In the case of alkyne insertion in to Pt–H bond of **1,** the nature of the substituents at the triple bond seems to play a crucial role. Preliminary results indicate that treatment of **1a** with DMAD affords indeed a mixture of isomers with *E*- and *Z*-stereochemistry about the alkenyl ligand [21].

2.3. Reactivity of *3* towards isocyanides

In the presence of stoichiometric amounts of *t*-butyl- or 2,6-xylylisocyanide, the dative Pt–OMe bond of **3a,b** was instantaneously broken and the yellow adducts $[(OC)_3Fe\{Si(OMe)_3\}(\mu\text{-}Ph_2PXPPh_2)Pt(CNR)\{C(CF_3){=}C(H)CF_3\}]$ (**4a** R = *t*-Bu, X = CH_2; **4b** R = 2,6-xylyl, X = CH_2; **4c** R = 2,6-xylyl, X = NH), were isolated as air-stable yellow solids (Scheme 2). In addition to the three *ν*(CO) stretches of the $Fe(CO)_3$-unit, the IR spectra of **4a/4b** display a strong *ν*(C≡N) vibration at 2221/2191 cm^{-1}, consistent with a terminal bonding mode of the isocyanide, ligated to the platinum centre. In the $^{19}F\{^1H\}$ spectrum of **4a** the resonances of the two trifluoromethyl substituents occur at δ −59.07 and −60.16. Both broadened signals show no resolved fine structure, however the observation of ^3J(Pt–F) coupling constant of 75 Hz for the first signal permits its assignment to the CF_3 group attached on the α-carbon. The supposed *E*-configuration of the CF_3-substituents about the alkenyl ligand (based on the proton-NMR data) was furthermore confirmed by an X-ray diffraction study performed on **4a**.

2.3.1. Crystal structure of $[(OC)_3Fe\{Si(OMe)_3\}(\mu\text{-}dppm)Pt(CN\text{-}t\text{-}Bu)\{C(CF_3){=}C(H)CF_3\}]$ *4a*

Suitable crystals of **4a** were grown from CH_2Cl_2/pentane. The molecular structure is depicted in Fig. 1(a), selected bond lengths and angles are given in Table 1. Since the overall geometry is quite reminiscent to that of the isocyanide-ligated acyl complex $[(OC)_3Fe\{Si(OMe)_3\}(\mu\text{-}dppm)Pt(CN\text{-}t\text{-}Bu)\{C(C{=}O)Me\}]$ [12], only the most pertinent structural features will be discussed. The metal–metal bond of **4a** is somewhat shorter than that of the acyl complex [274.66(11) vs. 279.8(2) pm]. The geometry around Pt is best described as distorted square planar, the root mean square deviation from the plane fitted through P(2)–C(7)–Pt–C(12)–Fe being

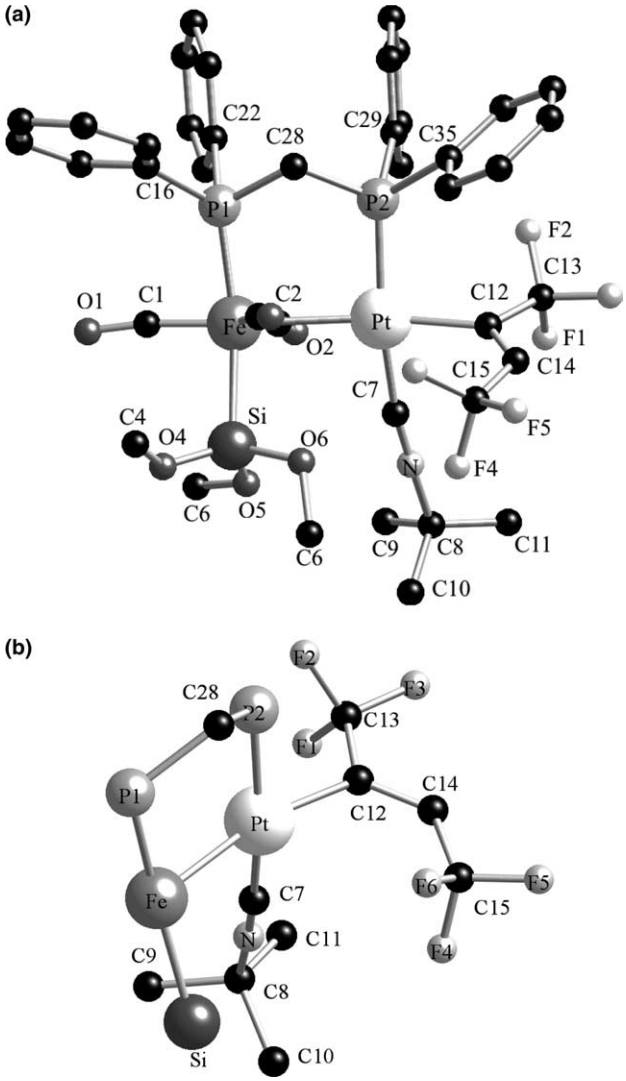

Fig. 1. (a) View of the molecular structure of **4a** with the numbering scheme. (b) View of the core structure of **4a** along the Fe–Pt bond.

Table 1
Selected bond lengths (pm) and bond angles (°) of **4a**

Bond lengths			
Fe–Pt	274.66(11)	Fe–Si	230.3(2)
Pt–P(2)	228.01(19)	Fe–C(1)	177.2(8)
Pt–C(7)	196.2(8)	Fe–C(2)	177.7(8)
Pt–C(12)	205.4(7)	Fe–C(3)	177.5(8)
C(12)–C(14)	133.0(11)	C(7)–N	115.9(9)
Fe–P(1)	222.4(2)	C(12)–C(13)	150.1(12)
Bond angles			
C(7)–Pt–C(12)	84.2(3)	C(3)–Fe–Si	81.3(2)
C(7)–Pt–P(2)	166.9(2)	C(1)–Fe–P(1)	90.6(2)
C(12)–Pt–P(2)	92.5(2)	C(2)–Fe–P(1)	104.2(2)
C(7)–Pt–Fe	96.0(2)	C(3)–Fe–P(1)	89.1(2)
C(12)–Pt–Fe	165.1(2)	Si–Fe–P(1)	165.92(8)
P(2)–Pt–Fe	90.42(5)	C(1)–Fe–Pt	169.5(2)
C(1)–Fe–C(2)	103.6(4)	C(2)–Fe–Pt	66.6(2)
C(1)–Fe–C(3)	110.0(3)	C(3)–Fe–Pt	78.8(2)
C(2)–Fe–C(3)	143.7(3)	Si–Fe–Pt	92.93(6)
C(1)–Fe–Si	83.0(2)	P(1)–Fe–Pt	95.40(6)
C(2)–Fe–Si	89.5(2)	N–C(7)–Pt	169.3(7)
C(7)–N–C(8)	176.6(8)	C(14)–C(12)–Pt	126.5(6)

0.232 Å. Notably the angles C(7)–Pt–P(2) [166.9(2)°] and Fe–Pt–C(12) [165.1(2)°] deviate from linearity. As can be seen in Fig. 1(b), this deformation has probably its origin in the steric repulsion between the $Si(OMe)_3$ group and the *t*-BuNC ligand, the torsion angle Si–Fe–Pt–C(7) being 29.72°. The alkenyl group occupies a position roughly perpendicular to the P(2)–C(7)–Pt–Fe plane, the C(15) trifluoromethyl substituent being orientated towards the $Fe(CO)_3$ moiety. The bond distance between the isocyanide carbon C(7) and Pt is slightly shortened compared to that found in $[(OC)_3Fe\{Si(OMe)_3\}(\mu\text{-dppm})Pt(CN\text{-}t\text{-}Bu)\{C(=O)Me\}]$ [196.2(8) vs. 198.9(8) pm]; despite the different character between a Pt–acyl and an Pt–alkenyl ligand, the Pt–C(acyl) and Pt–C(12) bond lengths are almost identical [205.6(8) vs. 205.4(7) pm]. A considerable shorter Pt-alkenyl bond length has been reported for the dimeric compound $[(PEt_3)Pt\{C(CF_3)=C(SnCl_3)CF_3\}(\mu\text{-Cl})]_2$ [198.2(6) pm] [22]. This divergence may be rationalized by the known *trans*-influence exerted by a metal–metal bond, thus elongating the Pt–C(12) bond in the case of **4a**. The molecular structure of **4b** has also been determined by us. Because of the insufficient data quality, we will however not discuss the structural features in detail. The crystallographic data corroborate at least, in line with the spectroscopic data and elemental analysis, the *E*-stereochemistry of the CF_3 substituents about the Pt–alkenyl ligand and the existence of a hydrogen-interaction between one molecule of $O{=}PPh_3$ and the N–H function of the μ-dppa back-bone [23].

Surprisingly, no spectroscopic change was noticed upon exposing a solution of **3a** under a CO atmosphere for 3h, excluding formation of $[(OC)_3Fe\{Si(OMe)_3\}(\mu\text{-dppm})Pt(CO)\{C(CF_3)=C(H)CF_3\}]$ (Scheme 3). Note that the alkenyl derivative $[(OC)_3Fe\{\mu\text{-}Si(OMe)_2(OMe)\}(\mu\text{-dppm})Pt\{C(Ph)=CH_2\}]$ afforded under identical conditions the CO adduct $[(OC)_3Fe\{Si(OMe)_3\}(\mu\text{-dppm})Pt(CO)\{C(Ph)=CH_2\}]$ [15]. This inertness in the case of **3a** may be explained by a strengthening of the dative Si–O → Pt bond due to the more electron-withdrawing propensity of $C(CF_3)=C(H)CF_3$ vs. $C(Ph)=CH_2$.

2.4. Formation and reactivity of $[(OC)_3Fe(\mu\text{-dppm})(\mu\text{-}CF_3C{=}CCF_3)Pt(CO)]$ 5

Unexpectedly, dichloromethane solutions of **3a** transformed (in a reproducible manner) within some days into the yellow alkyne-bridged compound $[(OC)_3Fe(\mu$-

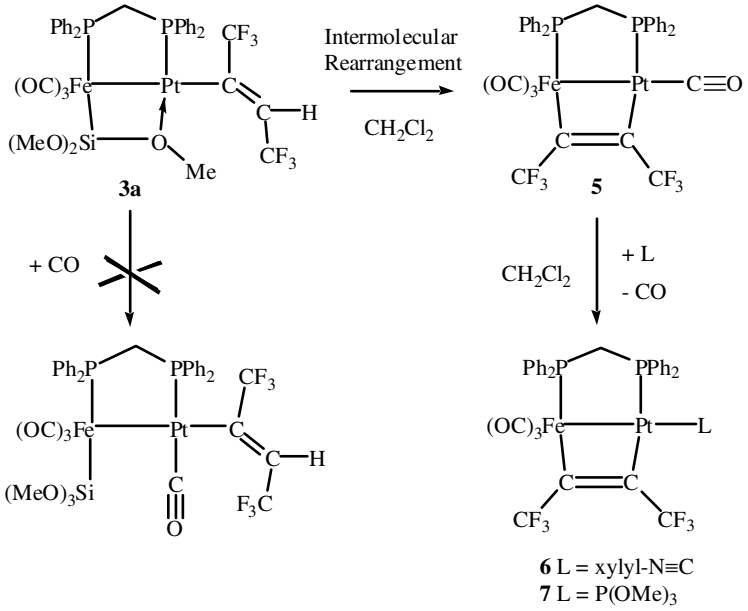

Scheme 3.

dppm)(μ-$CF_3C{=}CCF_3$)Pt(CO)] **5** (Scheme 3). The presence of a Pt-bound carbonyl ligand is evidenced from the IR spectrum, which displays in addition to three distinct terminal Fe–CO vibrations a fourth *ν*(CO) band at 2062 cm^{-1}. This additional carbonyl must stem from an intermolecular rearrangement reaction. At present, we have no satisfying hypothesis to account for this σ-alkenyl–μ-alkyne transformation and trapping of a carbonyl ligand. Slow cleavage of a Fe–$Si(OR)_3$ or Pt–$Si(OR)_3$ bond of bimetallic Fe–Pt complexes in halogenated solvents under exposure to day light or by addition of electrophiles has been encountered in previous work [24,25].

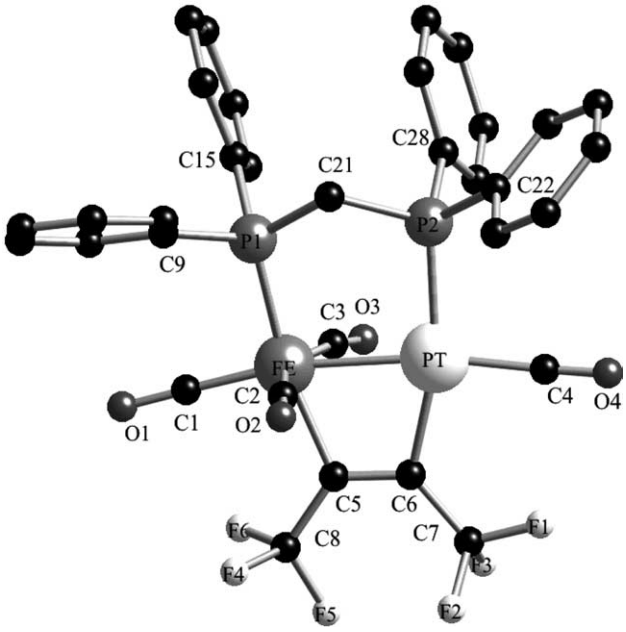

Fig. 2. View of the molecular structure of **5** with the numbering scheme.

The phosphane-induced σ-alkenyl–μ-vinylidene rearrangement shown in Scheme 1 represents another example of a Fe–SiR_3 cleavage reaction [15]. The inertness of **3a** towards CO (see above) makes an involvement of free carbon monoxide unlikely, therefore this additional carbonyl must stem from an intermolecular transfer reaction.

After addition of nucleophiles such as xylylisocyanide or trimethylphosphite, exclusively the Pt-bound carbonyl ligand of **5** is displaced affording the stable derivatives [$(OC)_3$Fe(μ-dppm)(μ-$CF_3C{=}CCF_3$)Pt(CNxylyl)] **6** and [$(OC)_3$Fe(μ-dppm)(μ-$CF_3C{=}CCF_3$)Pt{$P(OMe)_3$}] **7**. Table 4 shows that within the series **5**–**7** the magnitude of the ^{2+3}J(P–P) coupling is considerably increased compared to that of the alkenyl complexes **3** and **4**, whereas the ^{1}J(Pt–P) coupling constant is less than the half. In the ^{31}P NMR spectra of **5** and **6** a trifluoromethyl group is coupled with the Pt-bound dppm-phosphorus, hence the doublet resonance exhibits an additional quartet splitting owing to a ^{4}J(P–F) coupling of 11 Hz.

*2.4.1. Crystal structures of [$(OC)_3$Fe(μ-dppm)-(μ-$CF_3C{=}CCF_3$)Pt(CO)] **5** and [$(OC)_3$Fe(μ-dppm)-(μ-$CF_3C{=}CCF_3$)Pt(CNxylyl)] **6***

Bimetallic Pt–Pt complexes spanned by a μ-C_4F_6 ligand are not uncommon [17,25–29]; to the best of our knowledge, there is however no precedent of a heterodinuclear Fe–Pt compound bridged by a μ-RC_2R alkyne. We therefore carried out crystal structure determinations on **5** $0.5 \cdot C_6H_6$ and **6** $0.5 \cdot CH_2Cl_2$. Views of the structures are shown in Figs. 2 and 3; selected bond lengths and angles are listed in Tables 2 and 3. The most salient feature is the spanning of the two metal centres by HFB in a μ-η^1:η^1 mode parallel to the metal–metal axis [30]. The conservation of the Fe–Pt bond in **5** and **6** follows from the metal–

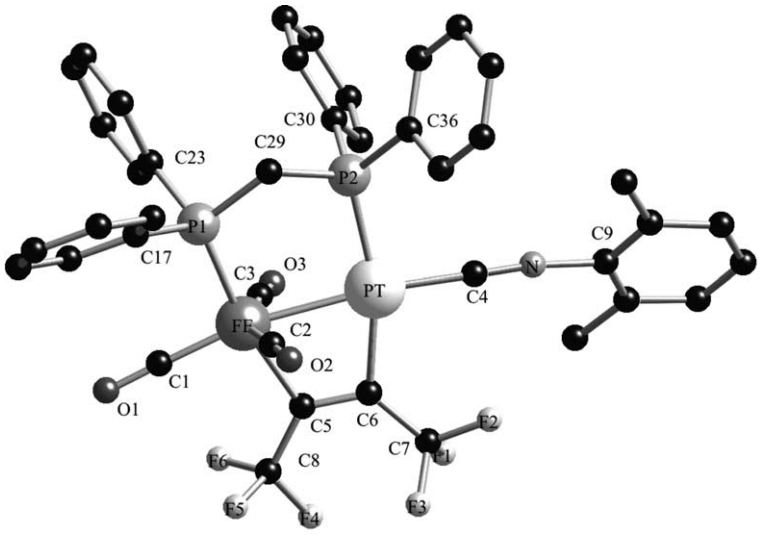

Fig. 3. View of the molecular structure of **6** with the numbering scheme.

Table 2
Selected bond lengths (pm) and bond angles (°) of **5**

Bond lengths			
Fe–Pt	260.85(12)	Fe–P(1)	224.0(2)
Pt–P(2)	229.35(19)	Fe–C(1)	176.4(8)
Pt–C(4)	190.3(8)	Fe–C(2)	178.4(8)
Pt–C(6)	206.2(8)	Fe–C(3)	179.6(9)
C(5)–C(6)	131.9(12)	Fe–C(5)	202.6(8)
Bond angles			
C(4)–Pt–C(6)	99.3(3)	C(3)–Fe–C(5)	82.2(3)
C(4)–Pt–P(2)	95.7(3)	C(1)–Fe–P(1)	94.0(3)
C(6)–Pt–P(2)	165.0(2)	C(2)–Fe–P(1)	89.3(3)
C(4)–Pt–Fe	171.0(3)	C(3)–Fe–P(1)	99.5(2)
C(6)–Pt–Fe	72.1(2)	C(5)–Fe–P(1)	167.1(2)
P(2)–Pt–Fe	92.94(5)	C(1)–Fe–Pt	169.1(3)
C(1)–Fe–C(2)	101.6(4)	C(2)–Fe–Pt	79.3(2)
C(1)–Fe–C(3)	102.6(4)	C(3)–Fe–Pt	74.8(3)
C(2)–Fe–C(3)	153.5(4)	C(5)–Fe–Pt	71.1(2)
C(1)–Fe–C(5)	98.1(4)	P(1)–Fe–Pt	96.85(6)
C(2)–Fe–C(5)	83.9(3)	C(6)–C(5)–Fe	110.9(6)
C(5)–C(6)–Pt	105.9(6)	P(1)–C(21)–P(2)	110.3(3)

Table 3
Selected bond lengths (pm) and bond angles (°) of **6**

Bond lengths			
Fe–Pt	260.26(9)	Fe–P(1)	224.69(15)
Pt–P(2)	229.70(14)	Fe–C(1)	178.6(6)
Pt–C(4)	193.8(6)	Fe–C(2)	179.6(6)
Pt–C(6)	206.7(5)	Fe–C(3)	178.9(7)
C(5)–C(6)	131.5(8)	Fe–C(5)	203.4(5)
C(4)–N	114.7(7)		
Bond angles			
C(4)–Pt–C(6)	99.3(2)	C(3)–Fe–C(5)	82.4(2)
C(4)–Pt–P(2)	96.00(18)	C(1)–Fe–P(1)	93.04(19)
C(6)–Pt–P(2)	165.54(16)	C(2)–Fe–P(1)	88.29(19)
C(4)–Pt–Fe	169.75(17)	C(3)–Fe–P(1)	98.96(19)
C(6)–Pt–Fe	72.20(16)	C(5)–Fe–P(1)	168.41(16)
P(2)–Pt–Fe	92.34(4)	C(1)–Fe–Pt	168.91(18)
C(1)–Fe–C(2)	104.2(3)	C(2)–Fe–Pt	75.61(19)
C(1)–Fe–C(3)	102.9(3)	C(3)–Fe–Pt	76.08(19)
C(2)–Fe–C(3)	151.5(3)	C(5)–Fe–Pt	71.00(16)
C(1)–Fe–C(5)	97.9(2)	P(1)–Fe–Pt	98.04(5)
C(2)–Fe–C(5)	85.3(2)	C(6)–C(5)–Fe	110.7(4)
N–C(4)–Pt	177.1(5)	C(5)–C(6)–Pt	105.6(4)
C(4)–N–C(9)	172.0(7)	P(1)–C(29)–P(2)	111.5(3)

metal separations of 260.85(12) and 260.26(9) pm, which are significantly shorter than that of **4a** [274.66(11) pm]. The dihedral angle Fe–C(5)–C(6)–Pt of the resulting 4-membered metallacycle amounts just to 0.41°. The C=C bond lengths of the bridging alkyne [131.9(12) and 131.5(8) pm] parallel those reported for [(COD)Pt(μ-$CF_3C{=}CCF_3$)$_2$Pt(COD)] [130(2) pm] and [(Ph_2BzP)(OC)Pt(μ-$CF_3C{=}CCF_3$)$_2$Pt(CO)-($PBzPh_2$)] [131.6(5) pm] [25,28]. The geometry around Pt is approximately square planar, only the angle P(2)–Pt–C(6) of 165.0(2)° deviates significantly from linearity. The four ligands around Pt are almost coplanar, the root mean square deviation from the plane fitted through P(2)–C(4)–Pt–C(6)–Fe being only 0.028 Å.

Table 4
Selected $^{31}P\{1H\}$ and $^{195}Pt\{1H\}$ NMR data (δ in ppm and J in Hz)

Complex	$\delta(P_{Fe})$	$\delta(P_{Pt})$	^{2+3}J(P–P); ^{1}J(Pt–P); ^{2+3}J(Pt–P)	$\delta(^{195}Pt)$
2	57.3 d	4.9 d	41; 4898; 43	−2367 dm[a]
3a	53.2 d	0.2 d	43; 4801; 31	−2319 dm
3b[b]	104.9 d	42.2 d	44; 5124; 26	−2324 dm
4a	59.1 d	11.0 d	84; 3130; 63.5	−2728 dm[c]
4b	58.3 d	11.9 d	84; 3104; 64	
4c[d]	110.2 d	60.7 d	85; 3378; 68	
5	73.0 d	20.8 dq[e]	122; 2006; 121	−2378 dm
6	77.3 d	20.7 dq[f]	122; 2102; 103	−2457 dm
7[g]	75.1 dd	24.2 dm	113; 2084	

[a] ^{3}J(Pt–F) = 61 Hz, dm = doublet of multiplets.
[b] δ ($OPPh_3$) = 28.7.
[c] ^{3}J(Pt–F) = 75 Hz.
[d] δ ($OPPh_3$) = 29.5.
[e] ^{4}J(P–F) = 11 Hz.
[f] ^{4}J(P–F) = 11 Hz.
[g] δ ($P(OMe)_3$) = 120.6, t broad, J(P–P) = 19 Hz, J(Pt–P) = 5167 Hz.

3. Conclusion and perspectives

We have demonstrated that the stereochemistry about the alkenyl ligand in heterodinuclear Fe–Pt complexes, resulting from the hydrometallation of [$(OC)_3$-Fe{$Si(OMe)_3$}(μ-Ph_2PXPPh_2)Pt(H)(PPh_3)], depends in a sensible manner from the electronic propensity of the alkynes used for this reaction. Whereas terminal aromatic alkynes give rise to a *cis*-insertion product, HFB insertion affords vinyl complexes with an *E*-stereochemistry about the alkenyl group. Furthermore, the latter compound rearranges gradually in solution with formation of [$(OC)_3$Fe(μ-dppm)(μ-$CF_3C{=}CCF_3$)Pt(CO)], an unprecedented example of heterodinuclear Fe-Pt system bridged by an alkyne in a μ-η^1:η^1 mode. We are currently elucidating more in detail the mechanism and parameters (influence of solvent, temperature, daylight) of this intermolecular transformation. Moreover, we have examined the site-selectivity of this dimetallacylobutene compound towards nucleophiles such as isocyanides and phosphites. The ease of the displacement of the Pt-bound carbonyl ligand should also allow the coordination of metallophosphines of the type [$(OC)_n$M(η^1-Ph_2PXPPh_2)] (M = Fe, Cr, Mo, W). Future studies will show whether this strategy can be exploited for the assembly of heterometallic cluster compounds incorporating a μ^3-η^2-C_4F_6 unit [31].

4. Experimental

All reactions were performed in Schlenk-tube flasks under purified nitrogen. Solvents were dried and

distilled under nitrogen before use, toluene and hexane over sodium, dichloromethane from P_4O_{10}. IR spectra have been recorded on a Nicolet Nexus 470 spectrometer. Elemental C, H, N analyses were performed on a Leco Elemental Analyser CHN 900. The ^1H and $^{31}P\{^1H\}$ NMR spectra were recorded at 313.13 and 81.01 MHz, respectively, on a Bruker Avance 300 instrument, the ^{19}F NMR spectra at 283.6 MHz on a Bruker AC 300 spectrometer (referenced to $CFCl_3$). ^{29}Si-INEPT and $^{195}Pt\{^1H\}$ chemical shifts were measured on a Bruker ACP 200 instrument (39.76 and 42.95 MHz) and externally referenced to TMS and K_2PtCl_4 in water with downfield chemical shifts reported as positive. NMR spectra were recorded in pure $CDCl_3$, unless otherwise stated. The reactions were generally monitored by IR spectroscopy in the ν(CO) region. The alkynes and isocyanides were obtained commercially from Fluka or Aldrich.

4.1. Preparation of *[(OC)$_3$Fe{μ-Si(OMe)$_2$(OMe)}-(μ-dppm)Pt{C(CF$_3$)=CH$_2$}] (**2**)*

A solution of **1a** (502 mg, 0.5 mmol) in CH_2Cl_2 (30 ml) was frozen in liquid nitrogen and an excess of trifluoropropyne (2 mmol) was condensed in the tube. The mixture was then slowly warmed to room temperature. After 15 h, all volatiles were removed under reduced pressure. The orange-yellow residue was recrystallised from CH_2Cl_2/hexane. Yield: (411 mg, 88%). Anal. Calc. for $C_{34}H_{33}F_3FeO_6P_2PtSi$ (935.57): C, 43.65; H, 3.56. Found: C, 43.23; H, 3.22%. IR (CH_2Cl_2): ν(CO): 1972 s, 1910 vs, 1882 vs ν(C=C): 1610 w cm^{-1}. ^1H NMR: δ = 3.69 (s, 3H, SiOCH_3), 3.78 (s, 6H, SiOCH_3), 3.65–3.80 (m, 2H, PCH_2P, partially obscured by SiOMe), 4.91 (m, 1H, vinyl-H, ^3J(Pt–H) = 64 Hz), 6.01 (m, 1H, vinyl-H, ^3J(Pt–H) = 121 Hz), 6.98–7.89 (m, 20 H, phenyl). $^{29}Si\{H\}$ NMR: δ 16.75 (dd, ^2J(P–Si) = 34.5, ^3J(P–Si) = 4.4 Hz).

4.2. Preparation of *[(OC)$_3$Fe{μ-Si(OMe)$_2$(OMe)}-(μ-dppm)Pt{C(CF$_3$)=C(H)CF$_3$}] (**3a**)*

A slow stream of C_4F_6 was bubbled through a solution of **1a** (502 mg, 0.5 mmol) in CH_2Cl_2 (20 ml). After 6 h, all volatiles were removed under reduced pressure. The orange-yellow residue was recrystallised from toluene/pentane. Yield: (416 mg, 83%). Anal. Calc. for $C_{35}H_{32}F_6FeO_6P_2PtSi$ (1003.03): C, 41.89; H, 3.21. Found: C, 42.23; H, 3.23%. IR (CH_2Cl_2): ν(CO): 1982 s, 1922 vs, 1898 vs ν(C=C): 1601 w cm^{-1}. ^1H NMR: δ = 3.60 (d, 3H, SiOCH_3, ^3J(Pt–H) = 21, ^4J(P–H) = 2 Hz), 3.70 (s, 3H, SiOCH_3), 3.72 (s, 3H, SiOCH_3), 3.77 (m, 1H, PCH_AP), 3.89 (m, 1H, PCH_BP), 6.49 (m, 1H, vinyl-H, ^3J(Pt–H) = 116 Hz), 6.48–7.84 (m, 20H, phenyl). $^{29}Si\{H\}$ NMR: δ 15.26 (dd, ^2J(P–Si) = 35, ^3J(P–Si) = 5 Hz).

4.3. Preparation of *[(OC)$_3$Fe{μ-Si(OMe)$_2$(OMe)}-(μ-dppa)Pt{(CF$_3$)=C(H)CF$_3$}] · O=PPh$_3$ (**3b**)*

A slow stream of C_4F_6 was bubbled through a solution of **1b** (502 mg, 0.5 mmol) in CH_2Cl_2 (20 ml). After 6 h, all volatiles were removed under reduced pressure. The orange-yellow residue was recrystallised from CH_2Cl_2/pentane. Yield: (276 mg, 43%). Anal. Calc. for $C_{34}H_{31}F_6FeNO_6P_2PtSi \cdot O{=}PPh_3$ (1004.56 + 278.29): C, 48.68; H, 3.61; N, 1.09. Found: C, 47.71; H, 3.33, N, 1.06%. IR (KBr)ν(NH···O) 3200 w, br, 2δ (NH) 2648 w, br; (CH_2Cl_2): ν(CO): 1984 s, 1914 vs, br ν(C=C): 1608w cm^{-1} [32]. ^1H NMR: δ = 3.58 (d, 3H, SiOCH_3, ^3J(Pt–H) = 21, ^4J(P–H) = 2 Hz), 3.67 (s, 6H, SiOCH_3), 4.60 (m, 1H, NH, ^3J(Pt–H) = 119 Hz), 6.6 (m, 1H, vinyl-H, ^3J(Pt–H) = 107 Hz), 6.94–7.89 (m, 35H, phenyl). $^{29}Si\{H\}$ NMR: δ 13.84 (dd, ^2J(P–Si) = 40, ^3J(P–Si) = 6 Hz).

4.4. Preparation of *[(OC)$_3$Fe{Si(OMe)$_3$}-(μ-dppm)Pt(CN-t-Bu){(CF$_3$)=C(H)CF$_3$}] (**4a**)*

t-BuNC (25 μL, 0.22 mmol) was added to a solution of **3a** (201 mg, 0.2 mmol) in CH_2Cl_2 (10 ml). The yellow solution was stirred for 10 min at ambient temperature, then all volatiles were removed under reduced pressure. The orange-yellow residue was recrystallised from toluene/pentane. Yield: (172 mg, 73%). Anal. Calc. for $C_{40}H_{41}F_6FeNO_6P_2PtSi \cdot C_7H_8$ (1086.71 + 92.14): C, 47.88; H, 4.19; N 1.19. Found: C, 47.73; H, 4.23; N, 1.28%. IR (CH_2Cl_2): ν(C≡N) 2221 s ν(CO): 1969 s, 1903 vs, 1879 vs ν(C=C): 1592w cm^{-1}. ^1H NMR: δ = 1.47 (s, 9H, *t*-Bu), 3.59 (s, 9H, SiOCH_3), 3.85 (m, 1H, PCH_AP), 4.03 (m, 1H, PCH_BP), 6.39 (m, 1H, vinyl-H, ^3J(Pt–H) = 120 Hz), 6.94–7.68 (m, 20H, phenyl).

4.5. Preparation of *[(OC)$_3$Fe{(OMe)$_3$}-(μ-dppm)Pt(CN-xylyl){(CF$_3$)=C(H)CF$_3$}] (**4b**)*

2,6-xylylisonitrile (13 mg, 0.1 mmol) was added to a stirred solution of **3a** (100 mg, 0.1 mmol) in CH_2Cl_2 (5 mL). After 15 min, the volume was reduced to 3 ml. Yellow crystals were obtained by layering with hexane. Yield: (68 mg, 61%). Anal. Calc. for $C_{43}H_{41}F_6FeNO_6P_2PtSi$ (1122.77): C, 46.00; H, 3.68; N, 1.25. Found: C, 45.79; H, 3.31; N, 1.06%. IR (CH_2Cl_2): ν(C≡N) 2192s ν(CO): 1975s, 1906vs, 1982s, ν(C=C): 1616w cm^{-1}. ^1H NMR: δ = 2.44 (s, 6H, xylyl-CH_3), 3.42 (s, 9H, SiOCH_3), 3.79 (m, 1H, PCH_AP), 4.13 (m, 1H, PCH_BP), 6.40 (m, 1H, vinyl-H, ^3J(Pt–H) = 121 Hz), 6.84–7.67 (m, 23H, phenyl).

Table 5
Crystallographic and refinement data for **4a**, **5** and **6**

	4a	**5** · $0.5C_6H_6$	**6** · $0.5CH_2Cl_2$
Formula	$C_{40}H_{41}F_6FeNO_6P_2PtSi$	$C_{36}H_{25}F_6FeO_4P_2Pt$	$C_{41.5}H_{32}ClF_6FeNO_3P_2Pt$
FW	1086.71	948.44	1055.01
T (K)	173(2)	173(2)	293(2)
Crystal size (mm)	$0.30 \times 0.20 \times 0.20$	$0.30 \times 0.20 \times 0.20$	$0.30 \times 0.20 \times 0.20$
Crystal system	Monoclinic	Triclinic	Monoclinic
Space group	$P2_1/c$	$P\bar{1}$	$P2_1/n$
Unit cell dimensions			
a (Å)	14.302(3)	12.254(3)	11.572(2)
b (Å)	11.174(2)	12.794(3)	17.298(3)
c (Å)	26.843(5)	13.408(3)	21.356(4)
α (°)	90	117.52(4)	90
β (°)	99.72(3)	97.24(3)	104.71(3)
γ (°)	90	99.91(3)	90
V (Å^3)	4228.2(14)	1784.9(7)	4134.8(13)
Z	4	2	4
ρ_{calc} (g cm^{-3})	1.707	1.765	1.695
μ (mm^{-1})	3.825	4.480	3.938
$F(000)$	2152	922	2068
θ Range (°)	2.33–25.00	2.47–26.00	1.54–25.00
Index ranges	$-17 \leqslant h \leqslant 17$, $-13 \leqslant k \leqslant 13$, $-30 \leqslant l \leqslant 31$	$-15 \leqslant h \leqslant 15$, $-15 \leqslant k \leqslant 15$, $-16 \leqslant l \leqslant 16$	$-13 \leqslant h \leqslant 13$, $0 \leqslant k \leqslant 20$, $0 \leqslant l \leqslant 25$
Collected reflections	29 284	11 288	7289
Independent reflections	7444	6540	7289
Data/restraints/parameters	7444/0/529	6540/0/444	7289/0/516
Largest differences in peak and hole (e Å^3)	1.490 and −2.966	3.037 and −2.532	0.670 and −0.613
Final R indices [$I > 2\sigma(I)$]	$R_1 = 0.0432$, $wR_2 = 0.1153$	$R_1 = 0.0494$, $wR_2 = 0.1232$	$R_1 = 0.0340$, $wR_2 = 0.0719$
R indices (all data)	$R_1 = 0.0595$, $wR_2 = 0.1220$	$R_1 = 0.0595$, $wR_2 = 0.1293$	$R_1 = 0.0512$, $wR_2 = 0.0839$
GOF on F^2	1.064	1.007	1.086

4.6. Preparation of [(OC)$_3$Fe{(OMe)$_3$}-(μ-dppa)Pt(CN-xylyl){(CF$_3$)=C(H)CF$_3$}] · O=PPh$_3$ (**4c**)

2,6-xylylisonitrile (13 mg, 0.1 mmol) was added to a stirred solution of **3b** · O=PPh$_3$ (128 mg, 0.1 mmol) in CH_2Cl_2 (8 ml). The orange-red solution was stirred for 10 min at ambient temperature, then the volume was reduced. Yellow crystals were obtained by layering with hexane. Yield: (91 mg, 63%). Anal. Calc. for $C_{61}H_{55}F_6FeN_2O_7P_3PtSi$ (1442.13): C, 50.80; H, 3.84; N, 1.94. Found: C, 50.79; H, 4.10; N, 1.97%. IR (CH_2Cl_2): *ν*(C≡N) 2189s *ν*(CO): 1980s, 1915vs, br *ν*(C=C): 1592w cm^{-1}. ^{1}H NMR: δ = 2.41 (s, 6H, xylyl-C*H*$_3$), 3.44 (s, 9H, SiOC*H*$_3$), 5.16 (m, 1 H, N*H*, ^3J(Pt–H) = 86 Hz), 6.46 (m, 1H, vinyl-H, ^3J(Pt–H) = 120 Hz), 6.94–7.82 (m, 38H, phenyl).

4.7. Preparation of [(OC)$_3$Fe(μ-dppm)-(μ-CF$_3$C=CCF$_3$)Pt(CO)] (**5**)

A CH_2Cl_2 solution of **3a** (501 mg, 0.5 mmol) was kept during 5 days in a Schlenk tube at ambient temperature, the progress of the transformation of **3a**–**5** was monitored by IR spectroscopy. Then all volatiles were removed under reduced pressure and the product separated from the residue by extraction with benzene. Pure **5** was obtained by layering with hexane in form of yellow crystals. Yield: (199 mg, 41%). Anal. Calc. for $C_{33}H_{22}F_6FeO_3P_2Pt \cdot 5C_6H_6$ (921.41 + 39.06): C, 47.25; H, 3.06. Found: C, 46.99; H, 2.99%. IR (CH_2Cl_2): *ν*(CO): 2062s, 2023s, 1971vs, 1950vs *ν*(C=C): 1607w cm^{-1}. ^{1}H NMR: δ = 3.81 (tr, 2H, PC*H* ^{2}P, ^2J(P–H) = 10.5, ^3J(Pt–H) = 43 Hz), 7.14–7.69 (m, 20H, phenyl).

4.8. Preparation of [(OC)$_3$Fe(μ-dppm)-(μ-CF$_3$C=CCF$_3$)Pt(CNxylyl)] (**6**)

XylylNC (15 mg, 0.11 mmol) was added to a stirred solution of **5** (95 mg, 0.1 mmol) in CH_2Cl_2 (8 ml). The yellow solution was stirred for 30 min at ambient temperature, and then the volume was reduced to ca. 3 ml. After layering with hexane, the air-stable yellow product crystallized. Yield: (79 mg, 75%). Anal. Calc. for $C_{41}H_{31}F_6FeNO_3P_2Pt \cdot 0.5\ CH_2Cl_2$ (1012.58 + 42.47): C, 47.25; H, 3.06; N, 1.33. Found: C, 46.99; H, 2.99; N, 1.29%. IR (CH_2Cl_2): *ν*(C≡N) 2153s *ν*(CO): 2009s, 1953vs, 1930vs *ν*(C=C): 1599w cm^{-1}. ^{1}H NMR: δ = 2.30 (s, 6H, C*H*$_3$), 3.79 (tr, 2H, PC*H*$_2$P, ^2J(P–H) = 10.5, ^3J(Pt–H) = 42 Hz), 7.03–7.69 (m, 23 H, phenyl).

4.9. Preparation of [(OC)$_3$Fe(μ-dppm)-(μ-CF$_3$C=CCF$_3$)Pt{P(OMe)$_3$}] (7)

P(OMe)$_3$ (26 μL, 0.22 mmol) was added to a stirred solution of **5** (190 mg, 0.2 mmol) in CH_2Cl_2 (15 ml). The yellow solution was stirred for 30 min at ambient temperature, and then the volume was reduced to ca. 5 ml. After layering with hexane, the air-stable product crystallized in form of yellow cubes. Yield: (157 mg, 78%). Anal. Calc. for $C_{35}H_{31}F_6FeO_6P_3Pt$ (1005.48): C, 41.81; H, 3.11. Found: C, 41.40; H, 3.01%. IR (CH_2Cl_2): *ν*(CO): 2002s, 1947vs, 1919vs *ν*(C=C): 1591w cm^{-1}. ^{1}H NMR: δ = 3.19 (d, 9H, OC*H*$_3$), 3.61 (m, 2H, PC*H* ^{2}P, not resolved), 7.13–7.65 (m, 35H, phenyl).

4.10. Crystal structure determinations

Data of **6** were collected on a Siemens AED2 diffractometer using graphite-monochromated Mo Kα radiation (λ = 0.71069 Å). The intensities were collected using $\Omega/2\theta$ scans, and the intensities of three standard reflections, which were measured after every 90 min, remained stable throughout the data collection. The intensities were corrected for Lorentz and polarization effects. An empirical absorption correction based on the Ψ-scans of three reflections was employed. Data of **4a** and **5** were collected on a Stoe IPDS diffractometer using graphite-monochromated Mo Kα radiation (λ = 0.71069 Å). The intensities were determined and corrected by the program INTEGRATE in IPDS (Stoe and Cie, 1999). An empirical absorption correction was employed using the FACEIT-program in IPDS (Stoe and Cie, 1999). The structures were generally solved by direct and Fourier methods using SHELXS-90. For each structure, the non-hydrogen atoms were refined anisotropically. All of the H-atoms were placed in geometrically calculated positions and each was assigned a fixed isotropic displacement parameter based on a riding-model. Refinement of the structures was carried out by full-matrix least-squares methods based on F_o^2 using SHELXL-97. All calculations were performed using the WINGX crystallographic software package, using the programs SHELXS-90 and SHELXL-97 [33]. The crystallographic data for each complex are gathered in Table 5.

Acknowledgement

We are grateful to the *Deutschen Forschungsgemeinschaft* and the French *Ministère de la Recherche et Technologie* for financial support.

Appendix A. Supplementary data

Crystallographic data for the structural analysis have been deposited with the Cambridge Crystallographic Data Centre, CCDC Nos. 249406–249408 for compounds **4a**, **5**, and **6**, respectively. Copies of this information may be obtained free of charge from: The director, CCDC, Union Road, Cambridge, CB2 IEZ,

UK (fax: +44-1223-336033; e-mail: deposit@ccdc.cam.ac.uk or www: http://www.ccdc.cam.ac.uk) Supplementary data associated with this article can be found, in the online version at doi:10.1016/j.jorganchem.2004.11.052.

References

[1] (a) For reviews dealing on heterobimetallics see: E. Sappa, A. Tiripicchio, P. Braunstein, Chem. Rev. 83 (1983) 202;
(b) B. Chaudret, B. Delavaux, R. Poilblanc, Coord. Chem. Rev. 86 (1988) 191;
(c) J.T. Mague, J. Cluster Sci. 6 (1995) 217;
(d) M.J. Chetcuti, Heterodinuclear Compounds, in: E.W. Abel, F.G.A. Stone, G. Wilkinson (Eds.), Comprehensive Organometallic Chemistry II, vol. 10, Pergamon, New York, 1995, pp. 23–84;
(e) P. Braunstein, J. Rosé, Catalysis and related reactions with compounds containing heteronuclear metal–metal bonds, in: E.W. Abel, F.G.A. Stone, G. Wilkinson (Eds.), Comprehensive Organometallic Chemistry II, Pergamon, Oxford, 1995, pp. 351–385;
(f) N. Wheatley, P. Kalck, Chem. Rev. 99 (1999) 3379;
(g) L.H. Gade, Angew. Chem. 112 (2000) 2768;
Angew. Chem., Int. Ed. Engl. 39 (2000) 2658;
(h) L.A. Oro, E. Sola, Mecanistic aspects of dihydrogen activation and catalysis by dinuclear complexes, in: M. Peruzzini, R. Poli (Eds.), Recent Advances in Hydride Chemistry, Elsevier, Amsterdam, 2001, pp. 299–327.

[2] (a) X.L.R. Fontaine, G.B. Jacobsen, B.L. Shaw, M. Thornton-Pett, J. Chem. Soc., Dalton Trans. (1988) 741;
(b) R. Boese, M. A: Huffma, K.P.C. Vollhardt, Angew. Chem., Int. Ed. Engl. 30 (1991) 1463.

[3] (a) D.S.A. George, R. McDonald, M. Cowie, Organometallics 17 (1998) 2553;
(b) S. Crementieri, P. Leoni, F. Marchetti, L. Marchetti, M. Pasquali, Organometallics 21 (2002) 2575;
(c) C.S. Chin, G. Won, D. Chong, M. Kim, H. Lee, Acc. Chem. Res. 35 (2002) 218.

[4] M.J.A. Kraakman, T.C.D. Koning, P.P.M.D. Lange, K. Vrieze, H. Kooijman, A.L. Spek, Inorg. Chim. Acta 203 (1993) 145.

[5] (a) M.J. Chetcuti, B.E. Grant, P.E. Fanwick, Organometallics 15 (1996) 4389;
(b) S. Tsutsuminai, N. Komine, M. Hirano, S. Komiya, Organometallics 23 (2004) 44.

[6] (a) M. Green, J.A.K. Howard, J. Simon, J. Porter, F.G.A. Stone, D.C. Tyler, J. Chem. Soc., Dalton Trans. (1984) 2553;
(b) I.J. Hart, F.G.A. Stone, J. Chem. Soc., Dalton Trans. (1988) 889.

[7] (a) A.M. Arif, D.J. Chandler, R.A. Jones, Organometallics (1987) 506;
(b) F.-E. Hong, I.-R. Lue, S.-C. Lo, C.-C. Lin, J. Organomet. Chem. 495 (1995) 97;
(c) For a recent exemple for a coupling reaction between HFB and 1,1-dimethylallene see:J.N.L. Dennett, J. Jacke, G. Nilsson, A. Rosborough, M.G. Ferguson, M. Wang, R. McDonal, J. Takats, Organometallics (2004) 4478.

[8] (a) R.E. Bichler, M.R. Booth, H.C. Clark, J. Organomet. Chem. 24 (1970) 145;
(b) P.G. Pringle, B.L. Shaw, J. Chem. Soc., Dalton Trans. (1983) 889;
(c) R.D. Adams, M. Huang, Organometallics 14 (1995) 2887.

[9] R. Regragui, P.H. Dixneuf, N.J. Taylor, A.J. Carty, Organometallics 9 (1990) 2234.

[10] J.D. King, M.J. Mays, C.-Y. Mo, P.R. Raithby, M.A. Rennie, G.A. Solan, T. Adatia, G. Conole, J. Organomet. Chem. 601 (2000) 271.

[11] (a) F.H. Antwi-Nsiah, O. Oke, M. Cowie, Organometallics 15 (1996) 506;
(b) B.D. Rowsell, R. McDonald, M.J. Ferguson, M. Cowie, Organometallics 22 (2003) 2944.

[12] M. Knorr, C. Strohmann, P. Braunstein, Organometallics 15 (1996) 5653.

[13] (a) B.T. Sterenberg, R.W. Hilts, G. Moro, R. McDonald, M. Cowie, J. Am. Chem. Soc. 117 (1995) 245;
(b) T.W. Graham, F.v. Gastel, R. McDonald, M. Cowie, Organometallics 18 (1999) 2177;
(c) J.E. Goldberg, J.A.K. Howard, H. Müller, M.U. Pilotti, F.G.A. Stone, J. Chem. Soc., Dalton Trans. (1990) 3055.

[14] (a) T. Yasuda, A. Fukuoka, M. Hirano, S. Komiya, Chem. Lett (1998) 29;
(b) S. Komiya, T. Yasuda, A. Fukuoka, M. Hirano, J. Mol. Cat. (2000) 63.

[15] M. Knorr, C. Strohmann, Eur. J. Inorg. Chem. (2000) 241.

[16] T.G. Appleton, H.C. Clark, R. Puddephatt, Inorg. Chem. 11 (1972) 2074.

[17] R. Puddephatt, M.A. Thomson, Inorg. Chem. 21 (1982) 725.

[18] (a) H.C. Clark, C.R. Jablonski, C.S. Wong, Inorg. Chem. 14 (1975) 1332;
(b) T.G. Attig, H.C. Clark, C.S. Wong, Can. J. Chem. 55 (1977) 189.

[19] H.C. Clark, C.S. Wong, J. Am. Chem. Soc. 99 (1977) 7073.

[20] D. Steinborn, S. Becke, C. Bruhn, F.W. Heinemann, J. Organomet. Chem. 556 (1998) 189.

[21] M. Knorr, I. Jourdain, unpublished results.

[22] H.C. Clark, G. Ferguson, A.B. Goel, B.L. Ruhl, Organometallics 3 (1984) 15.

[23] A hydrogen-interaction between O=PPh_3 and the N–H function of dppa has been crystallographically evidenced for [$(OC)_4Mo(\mu$-$SO_2)(\mu$-dppa)Pt(PPh_3)] · O=PPh_3: M. Knorr, C. Strohmann, Organometallics 18 (1999) 248.

[24] (a) P. Braunstein, M. Knorr, M. Strampfer, A. Tiripicchio, F. Ugozzoli, Organometallics 13 (1994) 3038;
(b) P. Braunstein, E. Colomer, M. Knorr, A. Tiripicchio, M. Tiripicchio-Camellini, J. Chem. Soc., Dalton Trans. (1992) 903;
(c) P. Braunstein, T. Faure, M. Knorr, Organometallics 18 (1999) 1791.

[25] (a) L.E. Smart, J. Browning, M. Green, A. Laguna, J.L. Spencer, F.G.A. Stone, J. Chem. Soc. Dalton Trans. (1977) 1777;
(b) N.E. Boag, M. Green, F.G.A. Stone, J. Chem. Soc., Chem. Commun. (1980) 1281.

[26] K.A. Azam, R.J. Puddephatt, Organometallics 2 (1983) 1396.

[27] G.J. Spivak, R.J. Puddephatt, J. Organomet. Chem. 551 (1998) 383.

[28] R. Ros, A. Tassan, R. Roulet, G. Laurenczy, V. Duprez, K. Schenk, J. Chem. Soc., Dalton Trans. (2002) 3565.

[29] For a μ-C_4F_6 ligand spanning a Fe–Fe bond in a trinuclear iron cluster see: R. Rumin, F.Y. Petillon, A.H. Henderson, L. Manojlovic-Muir, K.W. Muir, J. Organomet. Chem. 336 (1987) C50.

[30] This bonding mode may also be viewed as a dimetallated olefin (1,2-dimetallacyclobutene)..

[31] R.S. Dickson, G.D. Fallon, K.D. Heazel, M.J. Liddell, J. Organomet. Chem. 430 (1992) 221.

[32] (a) For a detailled discussion on the IR spectra and hydrogen bonding interactions of dppa see: J. Ellermann, G. Szucsanyi, K. Geibel, E. Wilhelm, J. Organomet. Chem. 263 (1984) 297;
(b) P. Bhattacharyya, R.N. Sheppard, A.M. Salwin, D.J. Williams, J.D. Woolins, J. Chem. Soc., Dalton Trans. (1993) 2393.

[33] (a) G.M. Sheldrick, SHELXL-97, Program for Crystal Structure Refinement. University of Göttingen, Germany;
(b) G.M. Sheldrick, SHELXS-90, Program for Crystal Structure Solution. University of Göttingen, Germany.